A Comprehensive Study on CO_2-Interphase Mass Transfer in Vertical Cocurrent and Countercurrent Gas-Liquid Flow

W.-D. DECKWER and I. ADLER

Institut für Technische Chemie der Technischen Universität Hannover, Callinstr. 3, 3000 Hannover 1, FRG

and

A. ZAIDI

Institut für Technische Chemie, Technische Universität Berlin, Straße des 17. Juni 135, 1000 Berlin 12, FRG

Cocurrent and countercurrent absorption and desorption of CO_2 in water was investigated in tall bubble columns (length 440 and 720 cm, diameter 15 and 20 cm, respectively). Operating conditions were applied which provided for high interphase mass transfer rates. Under these circumstances the relative gas holdup varies considerably with axial position whereas the mean bubble diameter measured at two points was found to be approximately constant. The measured data permit the calculation of local values of interfacial areas, superficial gas velocities, and frequency factors for bubble coalescence and break up.

A dispersion model which takes into account the hydrostatic head and a variable gas velocity was applied to describe the measured concentration profiles in both phases. If increased mass transfer coefficients at the column bottom and measured local values of the hold up were used a striking agreement between experimental and predicted profiles could be obtained. The findings lead to a more sophisticated picture of the complex behaviour of gas-liquid dispersions at high interphase mass transfer rates.

On a étudié, dans de hautes colonnes à bulles (longueur respective de 440 et 720 centimètres et diamètre respectif de 15 et 20 centimètres), l'absorption et la désorption de CO_2 dans l'eau, et ce dans le cas d'un écoulement dans le sens du courant et en sens contraire. On a employé des conditions d'opération qui permettaient l'obtention de taux élevés de transfert de masse entre les phases; dans ce cas, la rétention relative de gaz varie considérablement avec la position axiale; on a trouvé d'un autre côté que le diamètre moyen des bulles mesuré en deux points était approximativement constant. Les résultats des mesures permettent de calculer les valeurs locales des zones interfaciales, des vitesses superficielles du gaz et des facteurs de fréquence dans le cas de la coalescence des bulles et de leur rupture.

Pour décrire les profils de la concentration mesurée dans les deux phases, on a utilisé un modèle de dispersion qui tient compte de la tête hydrostatique et d'une vitesse variable du gaz. Si l'on employait des coefficients accrus de transfert de masse à la base des colonnes ainsi que les valeurs locales mesurées de la rétention, on pourrait obtenir une concordance remarquable entre les profils expérimentaux et ceux qu'on avait prévus. Les constatations mènent à une image plus subtile du comportement complexe des dispersions impliquant gaz et liquides à des taux élevés de transfert de masse entre les phases.

Owing to their simple construction and ease of performance bubble column reactors are widely used in industry. In addition to classical applications for carrying out chemical reactions the uses of bubble columns appear very promising in the field of *biotechnology*[1,2]. Recently completed comprehensive experimental studies with different synthetic media[3] and living microbial cells[4] proved that bubble columns are very appropriate for performing aerobic fermentation processes. Furthermore, Urza and Jackson[5] pointed out that tall bubble columns particularly provide for high oxygen transfer efficiencies. An economical evaluation also confirmed that tall bubble columns are advantageous in comparison with standard fermentation equipment[3,6].

Many studies on bubble columns have been published in the literature. However, the majority of the experimental results were obtained from operating conditions at which the applied concentrations of the transfer component are kept low.

Therefore the molar gas flow rate can be assumed as sufficiently constant. In addition, the columns commonly used are of laboratory scale and not as high that consideration of the pressure decrease along the column caused by reduced hydrostatic head would be necessary. Mass transfer data – k_La – obtained under such simplified conditions are frequently found to depend on column height and liquid flow rate[7-10]. However, it can easily be shown that the main parts of both dependencies are seemingly only, and are to be attributed to the application of the *NTU*-method which does not present a pertinent model for bubble columns[11,12,13].

The pertinent treatment of bubble column reactors should be based on the axial dispersion model[11,13-15]. Recently, a two-phase dispersion model for bubble columns of industrial size was proposed which accounts for variations of gas flow rate and pressure[17]. There it was demonstrated by numerical simulations that even at isobaric conditions the gas flow rate has to be considered as variable since gas

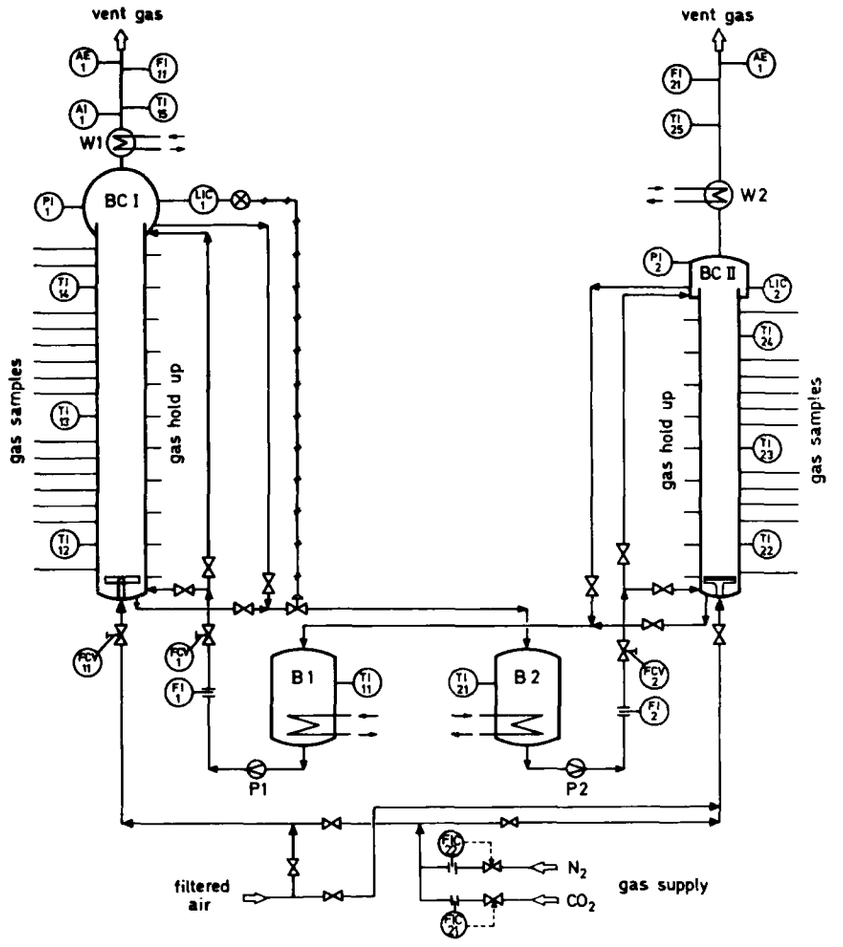

Figure 1 – Schematic presentation of experimental set up.

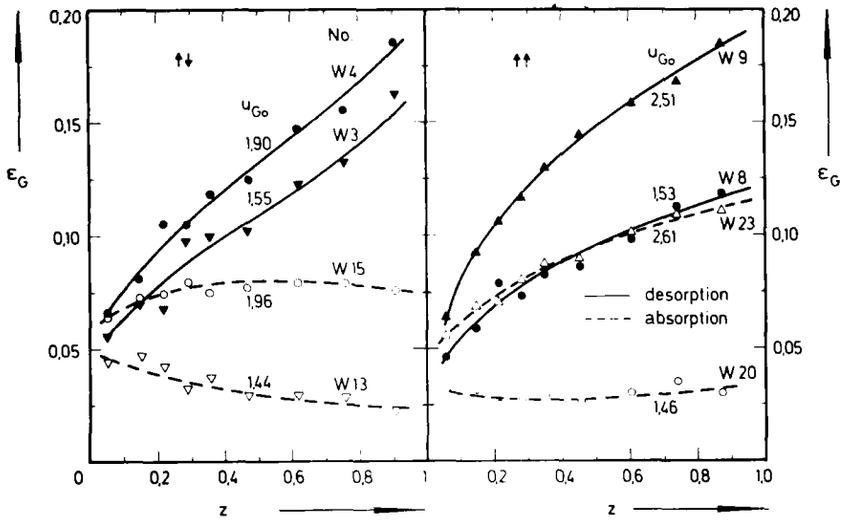

Figure 2 – Measured local values of relative gas hold up in BC I. $u_L = \pm 2.65$ cm/s.

volume decrease by absorption leads to increased gas residence time which in turn improves the conversion. Simpler models can be applied only if the column operates at elevated pressures and if, in addition, the gas shrinkage due to absorption is small.

Objective

When the absorption and reaction of isobutene in sulfuric acid was studied in a tall bubble column it was found that the conversions measured at the column exit could be explained reasonably only on the base of this improved model[18]. However, the comparison of experimental and predicted concentration profiles would present a better means to prove the validity of a particular model and to discriminate among rival models. Obvious experimental difficulties did not allow the determination of concentration profiles for the absorption and reaction of isobutene in sulfuric acid.

Therefore the physical absorption and desorption

TABLE 1

SIZES OF BUBBLE COLUMNS USED IN THIS STUDY

Column	Diameter cm	Length m	Gas sparger
BC I	20.	7.20	cross of nozzles (56) ϕ 1 mm
BC II	15.	4.40	glass sintered plate, ϕ 150 μm

of carbondioxide was investigated at cocurrent and countercurrent flow. Owing to the high CO_2 solubility operating conditions can be realized which lead to large interphase mass transfer flow rates. Therefore the CO_2-water system is thought to be very appropriate to simulate conditions which are encountered in industrial application of bubble columns as reactors. This paper presents very detailed results on the hydrodynamic properties and concentration profiles within bubble columns. Such findings have not been reported hitherto.

Experimental arrangement

The measurements were carried out in an experimental arrangement which is schematically presented in Figure 1. Two bubble columns (BC) which were made from glass (Schott & Gen., Maine) were used. Their geometrical sizes and the types of gas spargers are given in Table 1. The bubble columns were operated at cocurrent and countercurrent flow. For most measurements the liquid phase (tap water or aqueous solution of sodium sulfate 0.33 mol/ℓ) was recycled. The liquid flow rate was usually 3 m^3/h, but at lower liquid flow rates experiments were also carried out. The gas flow rate was varied from 0.9 to 7.5 m^3/h. (dry gas at 0°C, 101.325 kPa). For the majority of runs the experimental values of the inlet and outlet conditions are given in Tables 2, 3 and 4.

Both columns are equipped with numerous side flanges. A part of these were used to determine the gas hold up along the column using the manometric method. The interfacial areas were obtained from taking photograps of the gas-liquid dispersion. In *BC I* photographic pictures were taken at 350 and 610 cm above the gas distributor. In *BC II* the gas-liquid dispersion was photographed at 200 cm above column bottom. The bubble size distribution was obtained from the enlarged photographs by scaling about 500 bubbles. A particle size analyzer (Zeiss, TGA) was applied which classifies the bubbles in 48 sorts of different diameter. The interfacial area was calculated from the Sauter diameter of the bubble size distribution and the gas hold up.

Gas samples were withdrawn from the columns at several positions by using a special device which enabled to take samples without degasing of the liquid phase[19]. The gas samples were analyzed for CO_2 content by gas chromatography or absorption in *KOH* solution. To check the overall CO_2 balance the O_2 concentration was determined in the inlet and outlet gas. The CO_2 concentration in the liquid phase at column inlet and outlet was obtained from electrochemical methods. Also for some measurements the profile of the CO_2 concentration in the liquid phase was analyzed. A more detailed description of the arrangement of the columns and the applied analytical techniques is given elsewhere[19].

Fluid dynamic properties

Important fluid dynamic characteristics of gas-liquid dispersion occurring in contactors like bubble columns are the gas hold up ϵ_G, the bubble size distribution, the interfacial area and the mean bubble rise velocity. A number of correlations is available from the literature. For instance, correlations for ϵ_G were given in refs[3,22-24]. Unfortunately, the majority of the correlated data was obtained from operating conditions which are seldom found in industrial applications. The findings of this study indicate that the correlations given in the literature cannot reliably be applied to operating conditions which correspond to high interphase mass transfer rates. Obviously both mass transfer and pressure drop cause variations of the gas volume flow rate which in turn influence almost all fluid dynamic properties. To our knowledge detailed data on gas hold up, interfacial areas and bubble velocities obtained under such circumstances have not been reported hitherto.

Gas hold up

It is commonly assumed that gas hold up does not vary in the axial direction if one neglects entry and exit effects. This is indeed confirmed from measurements in relatively short columns and at conditions under which no appreciable mass transfer takes place[11,20]. However, in tall columns as used in this study the local gas hold up increases with column length due to volume expansion caused by decreasing hydrostatic pressure. The dependency of ϵ_G on z is more marked for case of desorption measurements since both pressure drop and mass transfer increase the hold up. This is shown in Figure 2 for some typical measurements at co- and countercurrent flow in *BC I*. One can discern that for the desorption runs the gas hold up may increase by 200 - 300 per cent when moving from the bottom towards the top of the column. On the other hand, for the absorption runs shown in Figure 2 ϵ_G may decrease, increase or is approximately constant. The behaviour depends on volume flow rates of the phases and the inlet concentration of CO_2 in the gas or liquid phase, respectively.

Figure 3 presents hold up data for absorption measurements in *BC II* where the gas was sparged by a sintered plate. Here minima can be observed which can be explained by the opposite effects caused by pressure decrease and mass transfer. In the lower part of the column absorption is large and ϵ_G may decrease. With increasing z the CO_2 content of the gas decreases, thus, absorption becomes negligible. Hence, ϵ_G increases again due to reduced hydrostatic head. Of course, the minima are particularly marked for countercurrent flow.

For the calculations presented below it is convenient to express the course of the gas hold up as a continuous function of z. The following form was chosen:

$$\epsilon_G(z) = \bar{\epsilon}_G \phi(z) \quad \ldots\ldots (1)$$

with

$$\phi(z) = a_o + a_1 z + a_2 z^2 \quad \ldots\ldots (2)$$

The coefficients, a_o, a_1 and a_2 were determined from the measured data by regression methods. $\bar{\epsilon}_G$ presents the integral or mean value of ϵ_G which is measured at the column bottom or calculated from the local data:

$$\bar{\epsilon}_G = \sum \epsilon_G(z_i)\, \Delta z_i \quad \ldots\ldots (3)$$

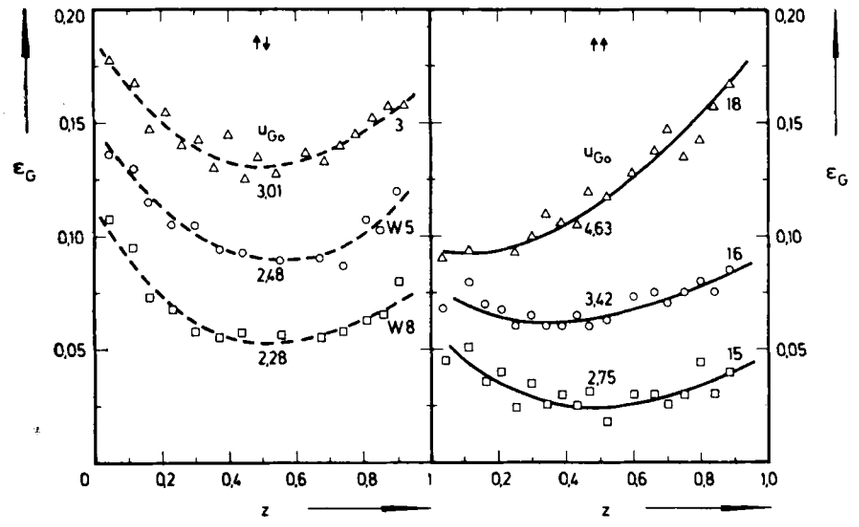

Figure 3 — Measured local values of relative gas hold up for absorption of CO_2 in BC II, $u_L = \pm 4.71$ cm/s.

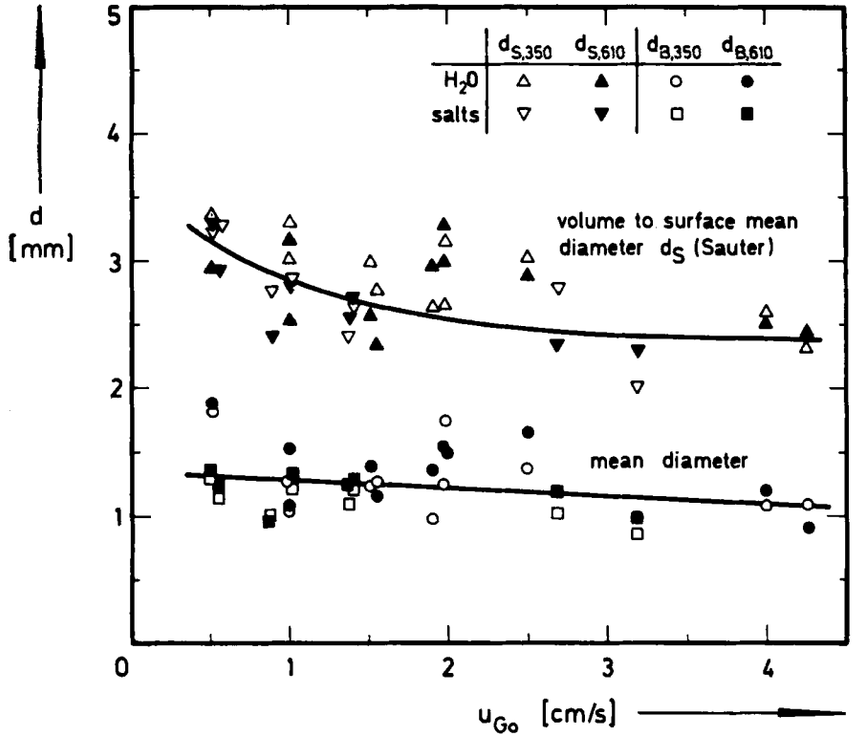

Figure 4 — Mean and Sauter diameter of the bubbles at a distance of 350 and 610 cm above the gas sparger, absorption and desorption runs, $u_L = \pm 2.65$ cm/s.

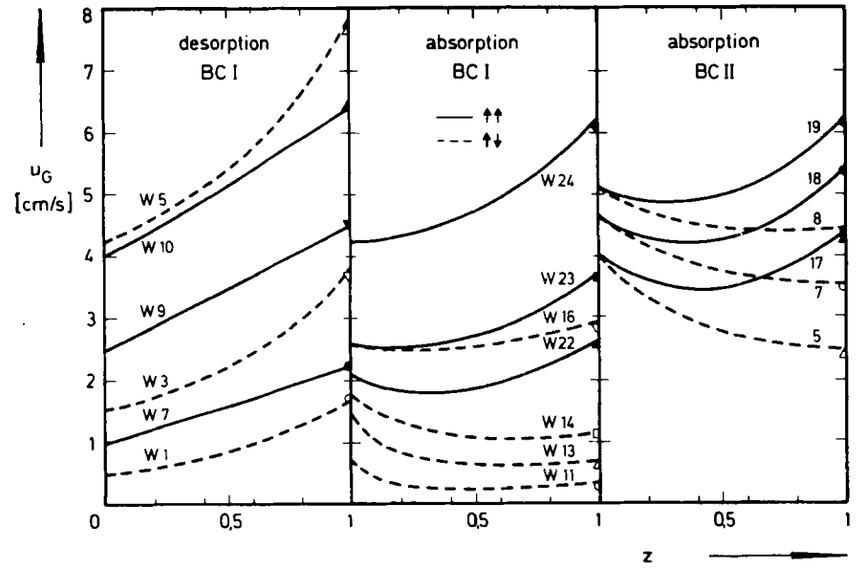

Figure 5 — Superficial gas velocity vs z (points at z = 1 refer to measured values).

TABLE 2

EXPERIMENTAL CONDITIONS FOR DESORPTION RUNS IN BC I
(W = water, S = sodium sulfate 0.33 mol/l), u_L = 2.65 cm/s, x_o = 0, T = 14°C

No.	flow	$\bar{u}_G$ cm/s	u_{G0} cm/s	u_{G1} cm/s	x_1	p_{Li} kPa	P_T kPa	$\bar{\epsilon}_G$	$k_L\bar{a}$ 1/s
*W*1	⇅	1.06	0.48	1.68	0.587	92.1	103.6	0.038	0.0045
*W*2		1.75	1.00	2.94	0.454	80.1	104.2	0.070	0.0081
*W*3		2.44	1.55	3.75	0.364	74.5	106.1	0.110	0.0129
*W*4		2.81	1.90	4.50	0.326	68.5	108.8	0.130	0.0147
*W*5		5.65	4.26	7.65	0.166	66.7	121.8	0.150	0.0170
*W*6	↑↑	1.11	0.50	1.60	0.510	97.7	104.3	0.032	0.0056
*W*7		1.89	1.00	2.63	0.391	89.2	106.2	0.060	0.0084
*W*8		2.66	1.53	3.55	0.326	88.2	107.3	0.089	0.0136
*W*9		3.95	2.51	3.95	0.238	81.5	111.1	0.138	0.0200
*W*10		5.79	4.00	7.20	0.170	77.4	118.3	0.155	0.0273
*S*1	⇅	1.13	0.53	1.62	0.564	99.6	104.3	0.032	0.0032
*S*2		1.66	0.88	2.25	0.468	101.5	107.4	0.056	0.0068
*S*3		1.85	1.14	2.43	0.390	87.2	107.0	0.074	0.0093
*S*4		2.23	1.39	2.98	0.374	101.9	111.4	0.092	0.0106
*S*5		3.77	2.53	4.90	0.302	101.0	110.2	0.151	0.0174
*S*6		3.58	2.68	4.20	0.177	66.8	117.6	0.165	0.0176
*S*7	↑↑	1.22	0.49	1.47	0.535	101.9	104.3	0.021	—
*S*8		2.11	1.01	2.70	0.419	102.6	106.3	0.053	—
*S*9		2.65	1.40	3.35	0.357	101.9	107.1	0.076	—
*S*10		5.13	3.19	5.37	0.232	101.2	114.2	0.153	—

TABLE 3

EXPERIMENTAL CONDITIONS FOR ABSORPTION RUNS IN BC I
(W = water), u_L = 2.65 cm/s. T = 14°C

No.	flow	$\bar{u}_G$ cm/s	u_{G0} cm/s	u_{G1} cm/s	x_0	x_1	P_{Li} kPa	P_T kPa	$\bar{\epsilon}_G$	$k_L\bar{a}$ 1/s
*W*11	⇅	0.33	0.71	0.30	0.755	0.122	13.6	101.6	0.013	0.0036
*W*12		0.66	1.05	0.65	0.651	0.142	15.7	102.6	0.025	0.0108
*W*13		0.83	1.44	0.78	0.747	0.196	15.8	101.9	0.032	0.0059
*W*14		1.23	1.77	1.13	0.694	0.232	13.7	102.3	0.049	0.0099
*W*15		1.72	1.96	1.72	0.561	0.205	14.8	102.3	0.076	0.0148
*W*16		2.64	2.58	3.06	0.423	0.204	12.5	104.0	0.120	0.0257
*W*19	↑↑	0.96	1.34	1.20	0.630	0.307	0.	101.8	0.027	0.0062
*W*20		1.00	1.46	1.25	0.665	0.338	0.	102.6	0.026	0.0060
*W*21		1.84	2.08	2.35	0.514	0.301	0.	102.7	0.055	0.0115
*W*22		2.25	2.01	2.91	0.227	0.128	0.	104.7	0.077	0.0145
*W*23		2.67	2.61	3.44	0.391	0.253	0.	105.9	0.098	0.0185
*W*24		4.70	4.23	5.91	0.255	0.276	0.	117.9	0.149	0.0312
*W*25		6.88	6.02	6.45	0.165	0.126	0.	129.2	0.154	0.0355

TABLE 4

EXPERIMENTAL CONDITIONS FOR ABSORPTION RUNS IN BC II,
WATER u_L = 4.72 cm/s, p_{Li} = O, T = 14° C

No.	flow	$\bar{u}_G$ cm/s	u_{G0} cm/s	u_{G1} cm/s	x_0	x_1	P_T kPa	$\bar{\epsilon}_G$	$k_L\bar{a}$ 1/s
1	⇅	0.58	1.63	0.55	0.756	0.0	105.0	0.027	0.0107
2		1.38	2.27	1.43	0.546	0.004	102.6	0.078	0.0221
3		1.71	3.34	1.45	0.692	0.014	102.2	0.099	0.0203
4		2.32	3.01	2.37	0.414	0.008	105.4	0.152	0.0335
5		2.83	4.01	2.40	0.569	0.042	106.0	0.178	0.0313
6		3.19	3.62	3.25	0.335	0.024	108.7	0.211	0.0310
7		3.79	4.63	3.52	0.481	0.102	109.5	0.193	0.0352
8		4.00	4.22	4.15	0.279	0.042	112.4	0.223	0.0285
9		4.49	5.09	4.53	0.415	0.140	113.9	0.186	0.0296
15	↑↑	0.69	1.64	0.75	0.766	0.274	102.0	0.017	0.0071
16		1.15	2.75	1.20	0.835	0.467	102.7	0.027	0.0119
17		2.20	3.42	2.49	0.673	0.377	103.9	0.072	0.0264
18		3.08	4.01	3.55	0.560	0.324	107.2	0.105	0.0396
19		3.94	4.63	4.59	0.478	0.293	109.6	0.126	0.0431
20		4.64	5.16	5.42	0.425	0.269	110.7	0.135	0.0490

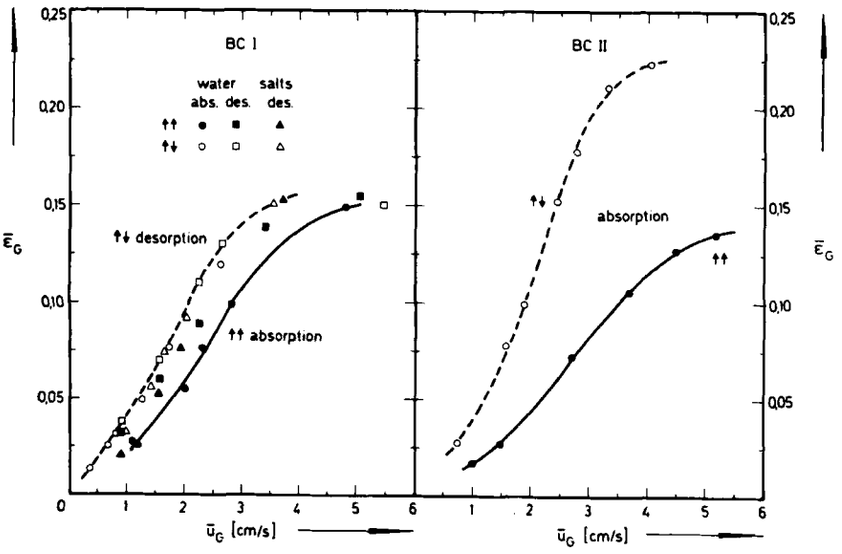

Figure 6 – Gas hold up vs gas velocity, integral values.

The $\bar{\epsilon}_G$-values are given in Tables 2, 3 and 4.

Pressure drop

If the gas hold up is constant, the pressure drop in bubble columns is linear:

$$P(z) = P_T [1 + \alpha (1 - z)] \quad \ldots\ldots (4)$$

where P_T is the pressure at top .α presents the ratio of maximum hydrostatic head to pressure at top:

$$\alpha = \frac{\rho g L (1 - \epsilon_G)}{P_T} \quad \ldots\ldots (5)$$

When $P(z)$ was calculated from the hold up data of our measurements it was found that P decreases almost linearly with z though ϵ_G is not independent of z. The reason for that is that integral values of ϵ_G have to be applied for calculating $P(z)$. Therefore, it is justifiable to use a linear pressure dependency in design calculations of bubble column reactors[11,17]. The deviation from linearity was less than 2 per cent for most runs of this study.

Bubble diameters and interfacial areas

The bubble size distributions determined in *BC I* at 350 cm and 610 cm above the gas sparger did not differ significantly, above all no systematic shift to larger diameters could be observed for the distributions determined from the 610 cm-position. From the size distributions of the bubbles the mean bubble diameter and the surface-to-volume mean bubble diameter (Sauter diameter) was calculated. They are plotted vs. the inlet gas velocity for the measurements in *BC I* in Figure 4. The superficial gas velocity at the top varies from 0.65 to 7.7 cm/s for these runs. The bubble size distributions are not symmetrical but are shifted to right. This is particularly the case for the distribution obtained from *BC I* which can be split into two symmetrical subcollectives[21]. The bimodal distributions explain the large differences between the Sauter diameter and the mean bubble diameter.

The data of Figure 4 show the important result that the mean diameter found in *BC I* at heights of 350 and 610 cm for water and electrolyte solutions can be regarded as approximately constant. Furthermore no difference was found for cocurrent and countercurrent flow and for absorption or desorption measurements. As the bubble diameter depends on the turbulence[25] within the dispersion the small decrease of the bubble diameter with increasing gas velocity can be attributed to increasing turbulence. For practical purposes it will, however, suffice to neglect this dependency on u_G and to use an average value of d_s from measurements at different gas velocities. Such average Sauter diameters found at a variety of conditions in *BC I* and *BC II* are compiled in Table 5. The data for oxygen interphase transfer in water and electrolyte solutions were taken from refs[12,26]. Though the applied systems and operating conditions vary considerably the Sauter diameters presented in Table 5 are very close to each other. Therefore it appears justifiable to conclude as a rule of thumb that in bubble columns of sufficient length and diameter the Sauter diameter of the bubbles does not significantly depend on the gas velocity, the gas distributor, the addition of electrolytes, the axial position, and the kind of operation (absorption - desorption, cocurrent - countercurrent flow). From all the data given in Table 5 one can calculate an average value of d_S which is 2.86 mm. This mean value of d_S will be considered in the following calculations.

From the Sauter diameter and the relative gas hold up the interfacial area can be calculated:

$$a = \frac{6\epsilon_G}{d_S} \quad \ldots\ldots (6)$$

Since d_S is independent on z one obtains with consideration of Equation (1)

$$a(z) = \frac{6\bar{\epsilon}_G}{d_S} \phi(z) \quad \ldots\ldots (7)$$

Thus, a depends on z in the same manner as the gas hold up.

Local dependency of the gas velocity

The amounts of O_2 and N_2 which are transferred from one phase to the other are very small and these components can therefore be regarded as inerts. Since in this study the gas phase profiles of CO_2 were measured it is possible to compute local values

TABLE 5

AVERAGE VALUES OF THE SAUTER DIAMETER FOR DIFFERENT SYSTEMS AND OPERATING CONDITIONS

column	system	operating conditions	number of data	average value of d_S, mm
BC I	CO_2/H_2O	abs./des./↑↑	15	2.91
		abs./des./↑↓	15	2.90
	CO_2/Na_2SO_4 (0.33 m)	des./↑↑	8	2.74
		des./↑↓	8	2.69
	O_2/H_2O	abs./des./↑↑	12	2.88
	O_2/Na_2SO_4 (.11/.35 m)	abs./↑↑	6	3.01
	$O_2/NaCl$ (.05-.60 m)	abs./↑↑	21	3.02
BC II	CO_2/H_2O	abs./↑↓	11	2.67
	O_2/H_2O	abs./des./↑↑	15	2.93
	O_2/Na_2SO_4 (0.11 m)	des./↑↑	5	2,53
	$O_2/NaCl$ (.05-.60 m)	des./↑↑	13	2.81

of the gas velocity by considering a balance on the inerts:

$$u_G(z) = u_{G_0} \frac{P_o\,(1 - x_o)}{P(z)\,(1 - x(z))} \quad \ldots\ldots (8)$$

Here again the point values of the gas phase mole fraction of CO_2 were smoothed and expressed as regression functions. As $P(z)$ is known from Equation (4) the local gas velocities could be calculated which are shown in Figure 5 for typical runs. For the case of desorption u_G increases as both mass transfer and pressure drop increase the gas volume flow rate. On the other hand, the gas velocity may run through a minimum for the case of absorption if the mole fraction of CO_2 in the inlet gas is large. In particular, this effect is marked in *BC II*. The points at $z = 1$ in Figure 5 refer to measured values of u_G at the column outlet. A striking agreement between the calculated and the experimental values can be observed. This confirms the consistency of the measured data.

From the axial gas velocity profiles we can now calculate the integral value of u_G which is given by

$$\bar{u}_G = \int_0^1 u_G(z)dz \quad \ldots\ldots (9)$$

Values of $\bar{u}_G$ are given in Tables 2, 3 and 4. The mean gas velocity $\bar{u}_G$ is used in Figure 6 to show the dependency of the integral gas hold up. One can discern from Figure 6 the usual relationship between ϵ_G and $\bar{u}_G$ for each series of runs. But the data reveal characteristic differences for cocurrent and countercurrent flow. The influence of the flow direction is particularly large in the smaller column (*BC II*) where the gas is sparged by a porous plate. In *BC I* the impact of the operating conditions is not as marked. Though the data scatter more than in *BC II* it can, however, be seen that for a given mean gas velocity the hold up increases in the following series: cocurrent absorption < cocurrent desorption < countercurrent absorption < countercurrent desorption.

Bubble coalescence and break up

A bubble balance over a volume element of the gas liquid dispersion yields for the bubble flux J:

$$-\frac{dJ}{dx} = k_C N_B - k_B N_B \quad \ldots\ldots (10)$$

N_B presents the bubble density (number of bubbles/cm³) which is given by

$$N_B(z) = \frac{\epsilon_G(z)}{\pi d_V^3/6} \quad \ldots\ldots (11)$$

When deriving Equation (10) it was supposed that the number of coalescences and break ups is proprotional to the bubble density N_B. k_C and k_B are frequency factors for coalescence and break up, respectively.

The presupposition that break up rates are proportional to the bubble density is analogous to chem-

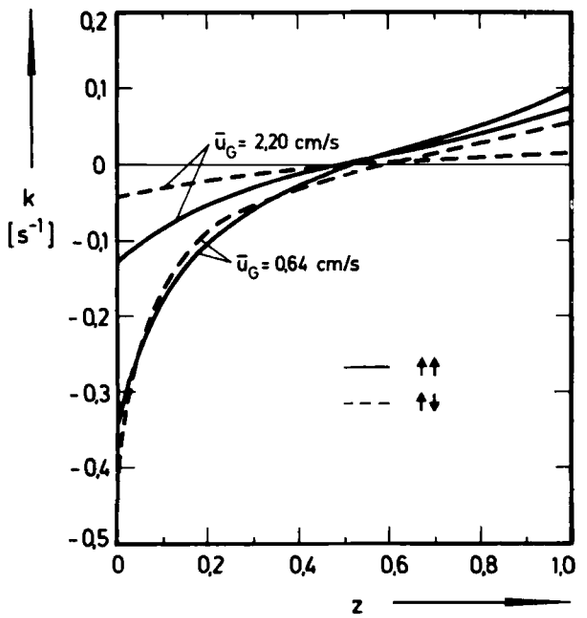

Figure 7 – Frequency factors for absorption runs in BC II.

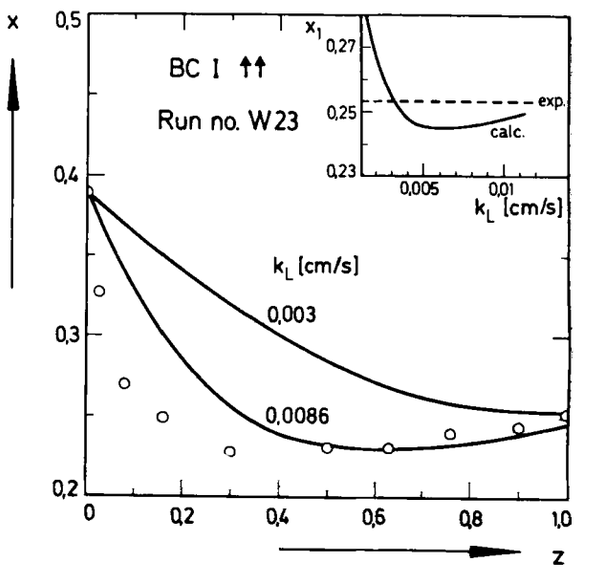

Figure 8 – Measured point values of CO_2 mole fraction compared with computed profiles using k_L-values which are constant along the column.

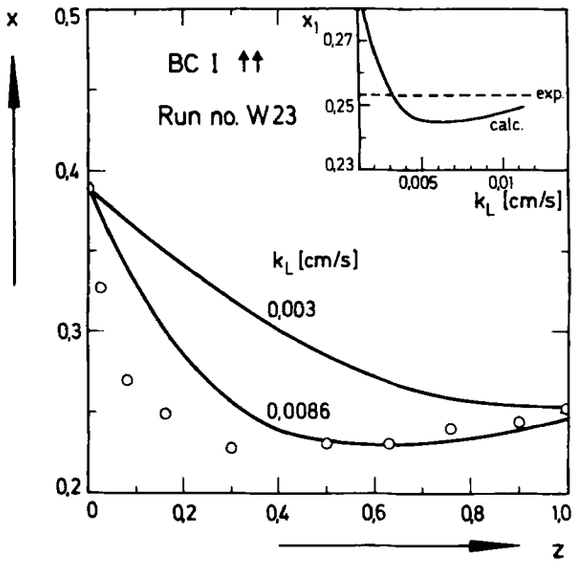

Figure 9 – Measured and predicted mole fraction of CO_2 in gas phase, $k_L \neq f(z)$.

ical kinetics for decomposition reaction which usually follow a first order law. On the other hand bubble coalescence involves several bubbles. Therefore the proportionality between coalescence rate and bubble density is certainly a coarse approximation only. It is, however, very convenient to work with this hypothesis which was also applied in[27,28].

Since the mean bubble diameter and the Sauter diameter do not depend on z it is reasonable to assume in Equation (11) that the volume diameter d_v is also constant. Introducing the bubble flux (number of bubbles/cm²s)

$$J(z) = \frac{u_G(z)}{\P\, d_V^3/6} \quad \ldots\ldots (12)$$

it follows

$$\frac{d\, u_G(z)}{dz} = kL\epsilon_G(z) \quad \ldots\ldots (13)$$

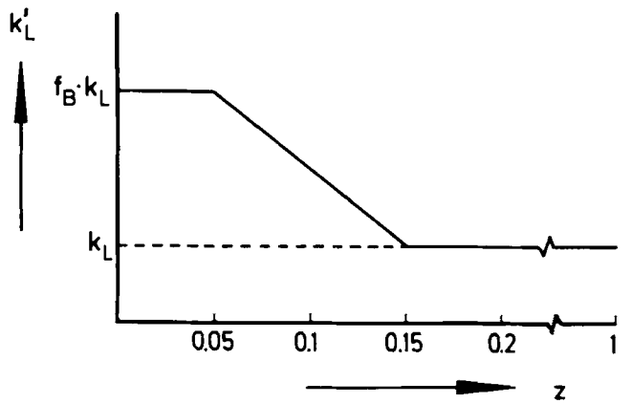

Figure 10 – k_L-profile used in computation, f_B is integer.

k is an overall frequency factor which is defined as

$$k = k_B - k_C \quad \ldots\ldots (14)$$

Using the measured data u_G and ϵ_G in Equation (13) can be expressed as regression polynomials in z. Then, local values of the frequency factor k can be calculated which are given in the following figures. For the desorption runs k is always positive. Of course, the number of bubble break ups is particularly large at the bottom for cocurrent flow and at the top for countercurrent flow, respectively. k-profiles for absorption runs in *BC II* are presented in Figure 7. One can discern therefrom that increased bubble coalescence takes place in the vicinity of the gas sparger where the interphase mass transfer is high. At these positions where the main part of the interphase mass transfer occurs the absolute values of the frequency factors are larger by at least an order of magnitude than for the condition of negligible interphase mass transfer[28]. It should, however, be emphasized that the frequency factors determined from Equation (13) do not permit any conclusion on the actual number of coalescences and break ups which lead to renewal and increased effectivity of the interfacial area. The value of k implies merely whether coalescence or break up predominates.

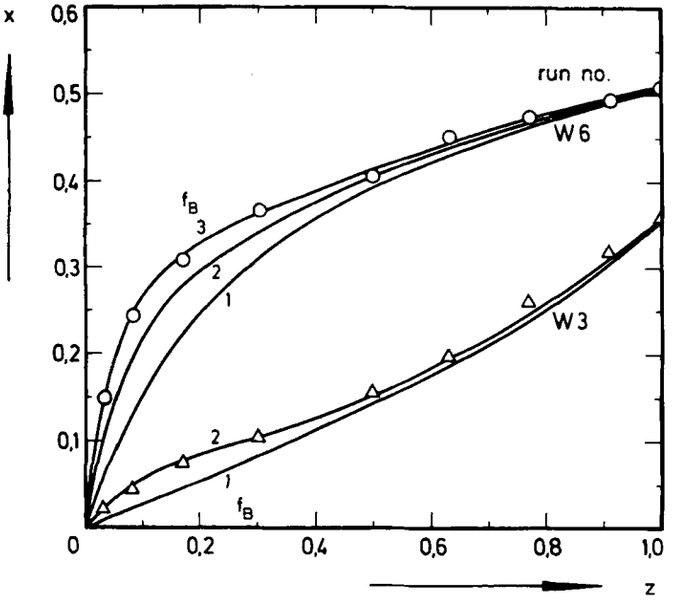

Figure 11 – Measured and calculated gas phase profiles for different values of f_B, BC I.

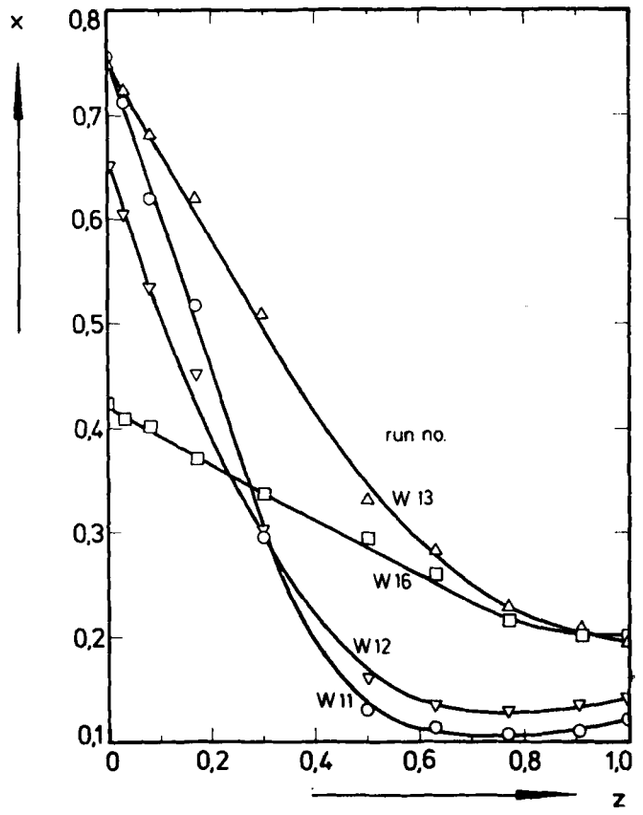

Figure 12 — Experimental and computed gas phase profiles for countercurrent absorption, BC I.

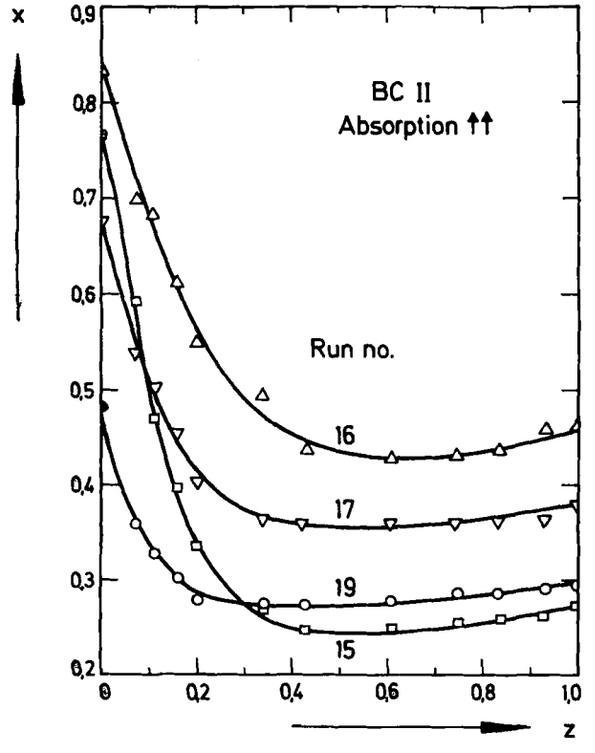

Figure 13 — Measured and computed liquid phase profiles, BC I.

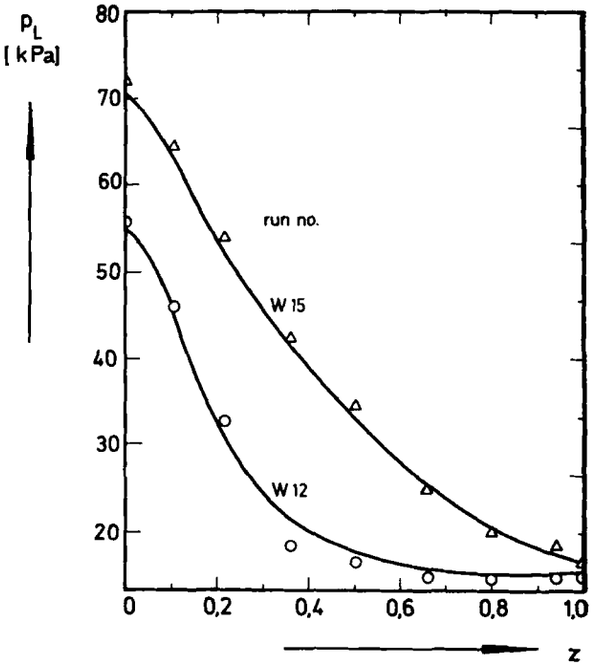

Figure 14 — Predicted and measured gas phase profiles for cocurrent absorption, BC II.

Mathematical model to describe the measured concentration profiles

From the findings on the fluid dynamic properties measured in bubble columns at conditions of high interphase mass transfer rates one arrives at a sophisticated picture of gas-liquid dispersions. Some more detailed results concerning the effect of electrolytes, the bubble size velocities, and an evaluation on the base of the "ideal bubbly flow"-concept[29] are presented elsewhere[30]. For the following description of measured concentration profiles by means of macroscopic balance equations it will suffice to state that most fluiddynamic properties turn out to be locally dependent. A remarkable exception presents only the bubble diameter if one does not consider entry and exit effects. No attempts were carried out to correlate the measured data as physico-chemical properties and geometrical sizes were not varied systematically and on the other side the most important correlation parameter namely the gas velocity is not constant along the column. Therefore the hold up profiles and the interfacial area will be considered in the model equations in form of the simple regression function, Equation (1), (2) and (7).

The evaluation of the experimental concentration profiles is based on the following assumptions

(1) Henry's law is valid

$$Px = Hc_L = p \quad \ldots\ldots (15)$$

(2) oxygen and nitrogen are inerts
(3) axial dispersion in liquid phase
(4) plug flow in gas phase
(5) neglect of radial dispersion effects
(6) pressure depends linear on z, Equation (4)
(7) gas hold up and interfacial area vary with z, Equations (1) and (7)
(8) gas velocity is variable, Equation (8)
(9) neglect of reaction of CO_2 with water
(10) mass transfer resistance is confined to liquid side
(11) isothermal operation

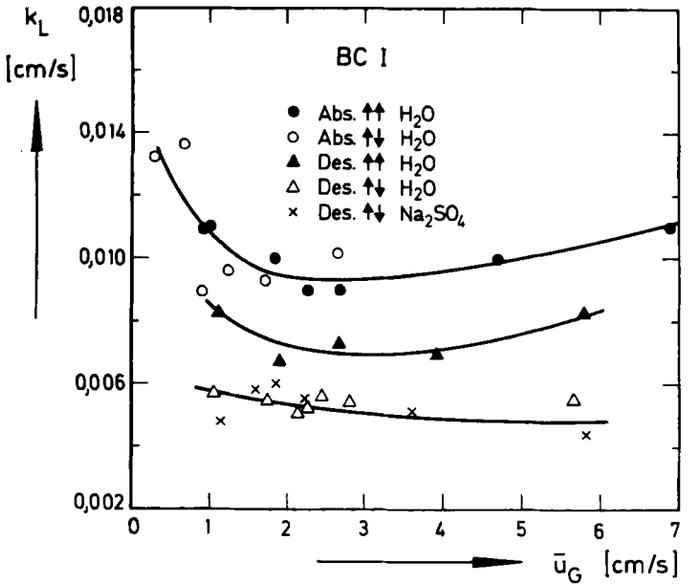

Figure 15 — Mass transfer coefficients k_L for different operating conditions in BC I.

Owing to the good agreement between measured and calculated outlet gas velocities (see Figure 5) the balance on the inerts is fulfilled which justifies assumption (2). The dispersion coefficients of the liquid phase were calculated from[11]:

$$D_L = 2.4\, d^{1.4}\, u_G^{0.3} \quad \ldots\ldots (16)$$

Equation (16) was established from measured data in the used columns and its significance was confirmed by other investigators[31,32]. The available information on gas phase dispersion coefficients[33] justifies assumption (4). The variations of pressure, hold up, interfacial area, and gas velocity are accounted for by the corresponding relations. From the dissociation constants it can be estimated that the ratio of hydrogencarbonate ions to dissolved CO_2 is about 0.003. Hence assumption (9) is fulfilled. As no reaction took place in the liquid phase and the gas concentrations are rather high (see tables 2 to 4) gas side resistances do not occur. Therefore assumption (10) is fulfilled. During the runs the temperature was measured along the columns at different locations. The largest measured difference was 0.5°C. Therefore the last assumption is justified also.

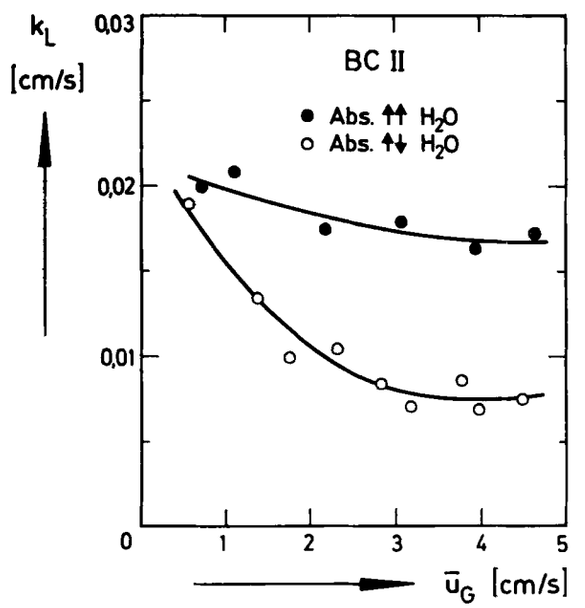

Figure 16 — Mass transfer coefficients for cocurrent and countercurrent absorption in BC II.

Model equations

The governing differential equations of the applied model are obtained from the mass balance over a volume element of length Δh. For the gas phase one obtains:

$$-\frac{d}{dh}\,(V_G c_G)\,\Delta h = k_L\,\Delta A (c_L^* - c_L) \quad \ldots\ldots (17)$$

Consideration of the ideal gas law, Henry's law and

$$V_G = Q\,u_G \quad \ldots\ldots (18)$$

$$\Delta A = a\,Q\,\Delta h \quad \ldots\ldots (19)$$

leads to

$$-\frac{d}{dh}\,(u_G\,Px) = k_L a\,\frac{RT}{H}\,(p_L^* - p_L) \quad \ldots\ldots (20)$$

In Equation (20) the liquid phase partial pressure of CO_2 ($p_L = Hc_L$) is introduced as this is a convenient measure of the CO_2 concentration in the liquid phase. Introduction of

$$z = h/L \quad \ldots\ldots (21)$$

$$p_L^* = Px \quad \ldots\ldots (22)$$

and substitution of the corresponding expressions for u_G, P and a, Equations (4), (7) and (8) yields by differentiating and rearranging:

$$\frac{dx}{dz} = -\,Sl_G\,\phi\,(z)\,(1-x)^2\left(\beta(z)x - \frac{p_L}{P_T}\right) \quad \ldots\ldots (23)$$

Here the following abbreviation are used:

$$Sl_G = k_L\,\frac{6\bar{\epsilon}_G}{ds}\,\frac{L}{u_{Go}\,(1+\alpha)\,(1-x_o)}\,\frac{RT}{H} \quad \ldots\ldots (24)$$

and

$$\beta(z) = 1 + \alpha(1-z) \quad \ldots\ldots (25)$$

The CO_2 liquid phase balance yields for the partial

pressure and with consideration of axial dispersion

$$\frac{1-\bar{\epsilon}_G\,\phi(z)}{Pe_L}\,\frac{d^2p_L}{dz^2}+\left(a^*-\frac{\bar{\epsilon}_G}{Pe_L}\,\frac{d\,\phi(z)}{dz}\right)\frac{dp_L}{dz}+St_L\phi(z)\,(P_T\beta(z)\,x-p_L)=0 \quad\ldots\ldots(26)$$

with

$$Pe_L=\frac{u_L L}{D_L} \quad\ldots\ldots(27)$$

and

$$St_L=k_L\,\frac{6\bar{\epsilon}_G}{d_s}\,\frac{L}{u_L} \quad\ldots\ldots(28)$$

If the phases flow countercurrently $a^*=1$ and for cocurrent flow $a^*=-1$. The initial condition for Equation (23) is

$$x(o)=x_o \quad\ldots\ldots(29)$$

The boundary conditions for Equation (26) are for the case of cocurrent flow ($a^*=-1$):

$$p_L(o)=p_{Li}+\frac{1-\bar{\epsilon}_G\phi(0)}{Pe_L}\,\frac{dp_L(o)}{dz} \quad\ldots\ldots(30)$$

$$\frac{dp_L(1)}{dz}=0 \quad\ldots\ldots(31)$$

and for countercurrent flow ($a^*=+1$):

$$\frac{dp_L(0)}{dz}=0 \quad\ldots\ldots(32)$$

$$p_L(1)=p_{Li}-\frac{1-\bar{\epsilon}_G\phi(1)}{Pe_L}\,\frac{dp_L(1)}{dz} \quad\ldots\ldots(33)$$

The index i refers to inlet conditions.

Owing to the consideration of a variable gas velocity the model equations are no more linear even for the case of physical mass transfer. The method of Lee[34] was used to solve the differential Equations (23) and (26). This solution procedure was found to be very convenient to solve the non-linear boundary value problem with non-constant coefficients[7,18].

As to Equation (16) the liquid phase dispersion coefficient depends on gas velocity and this may vary considerably along the column (see Figure 5). Therefore preliminary computations were carried out with different values of D_L calculated from u_{Go} and u_{G1}. These calculations revealed that computed gas phase profiles are practically not affected by D_L for the possible range of variation. Therefore D_L was calculated from Equation (16) using the mean gas velocity defined by Equation (9).

The liquid side mass transfer coefficient k_L is now the only quantity which is unknown. These k_L-values are important results of this study and it was thought that the k_L-data can be determined easily by fitting model predictions with various k_L-values to the experimental gas phase profiles. Therefore no special optimization procedure was applied. Since only one parameter had to be determined and the computations were fast enough a trial-and-error method was sufficient.

Description of measured profiles

Some typical results of attempting to match the measured profiles with a constant value of k_L are shown for cocurrent absorption runs in *BC I* in Figures 8 and 9. It can be discerned that it is not possible to describe the experimental profile over the whole column. In the graphs given at the right hand corners of Figures 8 and 9 the calculated outlet mole fractions of CO_2 are plotted vs. k_L. The calculated curves reveal flat minima which lie above or below the experimentally observed values. However, the measurements and the computations agree fairly well over an appreciable region of k_L if one considers that the measured outlet data are subject to experimental errors. The predicted outlet concentration is rather insensitive to large variations of k_L. Of course, this is partly caused by the physical equilibrium which will be established in the upper part of the tall column used for these cocurrent absorption runs. However, similar results were also obtained for other operating conditions and therefore one has to conclude that measuring only outlet concentrations will not yield unambiguous mass transfer data.

If larger k_L-values than those given in Figure 8 and 9 were used in the computations a solution of the model equations could not be attained. It is assumed that this behaviour is due to stiffness of the system of differential equations. It is, however, obvious that larger k_L-values than those used in Figures 8 and 9 are physically not realistic for the upper part of the column. Therefore a constant k_L is not able to describe the measured data. Hence a locally dependent mass transfer coefficient was applied. Several functions were tested to simulate a continuous k_L-profile. However, as the theoretical profiles indicate that mass transfer rates are too small merely near the gas distributor it suffices to apply increased k_L-values only there. Favorable and consistent results for all runs could be obtained if the constant mass transfer coefficient was replaced by a profile which is shown in Figure 10 and defined by the following equations:

$$\begin{aligned} k_L' &= f_B\,k_L && \text{when } 0\le z<0.05\\ k_L' &= k_L\,(1+10\,(f_B-1)\,(0.15-z)) && \text{when } 0.05\le z<0.15\\ k_L' &= k_L && \text{when } 0.15\le z\le 1 \end{aligned} \quad\ldots\ldots(34)$$

For reasons of simplification integer values of f_B were taken only.

The following figures demonstrate that application of this profile for k_L leads to a good agreement between model predictions (full drawn curves) and experimental results. Moreover the computations proved that f_B-values of 2 or 3 had to be used only. For the majority of the measurements the necessary value of f_B was two. Only for a few absorption and all the desorption runs at cocurrent flow a value of $f_B=3$ was needed in order to fit the experimental data. The effect of the local "enhancement" factor f_B on the calculated profiles can be discerned from Figure 11 for two desorption runs in *BC I*. A twofold (W3) or threefold (W6) increase of the mass transfer coefficient in the vicinity of the gas sparger yields an excellent description of the measured results.

The course of the mole fraction of CO_2 in the gas phase for absorption in *BC I* and *BC II* for countercurrent and cocurrent flow, respectively, is shown in Figures 12 and 14. The profiles are very steep if the gas velocity is low. For some runs in *BC I* CO_2-concentration profiles were also determined in the liquid phase applying electrochemical and/or titration methods. Two examples are plotted in Figure 13. Here p_L presents the partial pressure in the liquid phase. Once again the steepness of these profiles is remarkable. Of course, this is due in part to the

large Peclet numbers of the liquid phase resulting from the high liquid flow rate which was applied in this investigation. Such liquid concentration gradients present the final result of opposing effects, namely mass transfer and dispersion (and reaction). At high interphase mass transfer flow rates the dispersion flows may not be fast enough to equalize the concentration profile which is built up by mass transfer from the gas to the liquid phase.

It should be pointed out that such marked profiles as presented in the Figures 11 to 14 have not been reported hitherto. The gas phase profiles are marked and some of the absorption runs reveal a flat minimum value. Such extreme values in the gas mole fraction were not observed experimentally before, however, they were already predicted from numerical studies for the case of cocurrent flow of the phases[17] and can be explained by the decreasing hydrostatic head in the columns. For the countercurrent absorption runs in *BC I* the minimum results from the rather high inlet concentration of CO_2 in the liquid phase, see Table 3. Due to the hydrostatic head the concentration of CO_2 in the gas phase decreases to a lower value than that one which corresponds to the inlet partial pressure of the liquid phase. If therefore the phases flow countercurrently at the top of the column small amounts of CO_2 will desorb from the liquid phase which is supersaturated compared with gas phase. Of course, if the inlet concentration of CO_2 in the liquid phase is zero no minima will occur for countercurrent flow. Though the observed minima are irrelevant for any technical application they present a justification of the model applied in this paper and in refs[17,18] since simpler models are not able to describe the measured profiles.

Liquid side mass transfer coefficients

The k_L-values determined from matching theoretical predictions to experimental results are presented in Figures 15 and 16. The obtained k_L-data are in the reasonable range. However, enhanced mass transfer takes place in the region adjacent to the gas distribution system. Though this was not found explicitly before when studying mass transfer in all columns it can be suspected and appears quite reasonable as near the gas entry higher frequency factors for bubble coalescence and break up were found except for countercurrent desorption runs. It can be observed visually too that in the zone following the sparger the flow pattern is not uniform but strong turbulences occur. At a length of 0.5 to 1 m above the sparger a quasihomogeneous gas-liquid dispersion is formed which flows then rather uniformly towards the column top. Furthermore one has to consider that the lowest point where the bubble size distribution was measured was 350 cm above the sparger. Therefore the equilibrium bubble diameter will not be established in the vicinity of the gas distributor and smaller bubbles may occur there. As this would lead to higher interfacial areas the found increase in k_L may be seemingly only. Further studies are in preparation to clarify this point. For practical purposes as for instance a rough estimation of mass transfer efficiency the volumetric mass transfer coefficient k_La is usually applied. Mean k_La-values are given in Tables 2 to 4. They were calculated with k_L and a mean value of a obtained from $\bar{a} = 6\bar{\epsilon}_G/d_s$ with $d_s = 0.286$ cm.

It can be seen from Figures 15 and 16 that all kinds of measurements yield slightly increased mass transfer coefficients for the low gas velocities. The same result was obtained from studies on O_2-mass transfer reported in[11,12]. Using the arguments of Calderbank and Moo-Young[35] a possible explanation for the increased k_L-values at low gas velocities may be obtained from the following observations: At low gas throughputs the bubbles are slightly larger, they rise freely and rather independently from each other. Photographic pictures indicate that they oscillate and their shape varies permanently. Contrary to that behaviour bubbles do not move independently in systems of high bubble density corresponding to higher gas velocities. The gas-liquid dispersion appears then to be a close packing of rather rigid spheres. This supposition is supported by the fact that the bubble size distributions are much more narrow than for low gas velocities, see also ref[21]. Therefore, these observations may provide probably for a qualitative interpretation of decreasing mass transfer coefficients with increasing bubble densities.

From Figures 15 and 16 one can discern that the k_L-data for the absorption runs are considerably higher than the ones for desorption. Furthermore, cocurrent desorption in *BC I* and cocurrent absorption in *BC II* yields surprisingly higher values of k_L than for countercurrent flow. Additional measurements at different liquid flow rates indicate that a dependence on the slip velocity does not exist. Several attempts were carried out to find a reasonable and consistent quantitative relation between the k_L-values observed and the bubble densities, and/or the frequency factors for coalescence and break up. However, a simple and unmabiguous relationship could not be attained. Correlations proposed in the literature[3,22,35-38] were tested also to explain the dependencies of the k_L-data obtained on the operating conditions. Unfortunately it was found that all the correlations are not capable of interpreting the measured data. k_L- or k_La-data used for establishing correlations were commonly obtained at low mass transfer rates and evaluated on the base of the two limiting cases of the liquid phase behaviour i.e. the CSTR[22,36] or the CTR[7-10]. Both models are not appropriate to describe the hydrodynamic behaviour of the liquid phase in bubble columns[11-13]. Hence comparison with literature data is difficult. In addition, comparison and just so correlation of the obtained mass transfer coefficients appears not reasonable as at high interphase mass transfer important parameters like gas velocity and hold up are not constant along the columns. Correlations will be meaningful only if further data are available from studies of other systems but obtained at similar operating conditions.

Summary and conclusions

The results of this study reveal a complex behaviour of bubble columns if they are operated at conditions which lead to high interphase mass transfer rates. It is thought that the simple construction of bubble columns causes such complex hydrodynamic and mass transfer properties since no installments provide for a repeated redistribution of gas and liquid and no additional mechanical energy is introduced to the gas/liquid dispersion. Therefore a rather sophisticated model is needed to describe the performance of tall bubble column reactors.

The experimental concentration profiles confirm the significance of the applied model which accounts for the hydrostatic head and gas flow variations. However, the excellent agreement between experi-

mental and theoretical results could only be obtained with consideration of detailed information on the hydrodynamic properties. In addition and contrary to previous findings at low interphase transfer rates mass transfer coefficients differ largely for absorption and desorption measurements. The k_L-data may also depend on the direction of the flow of the liquid phase. Unfortunately exact knowledge of hydrodynamic properties will be seldom available. This fact will certainly not permit the widespread application of the proposed model in industry at the present time. Therefore further studies at operating conditions prevailing in industry are needed which are focused on measurements inside the equipment and which are evaluated on the base of realistic models. It can be expected that from such studies reasonable guidelines may be developed which provide for a more reliable design of bubble columns.

Acknowledgment

The authors gratefully acknowledge support from Deutsche Forschungsgemeinschaft and Stiftung Volkswagenwerk. Thanks are due to G. Zoll for help at performing and evaluating the measurements.

Notation

a = specific interfacial area
A = interfacial area
c = concentration
d = column diameter
d_s = volume-to-surface mean diameter, Sauter diameter
d_v = volume mean diameter
D_L = liquid phase dispersion coefficient, cm²/s
f_B = mass transfer enhancement factor, Equation (34)
g = gravitational acceleration
h = axial coordinate
H = Henry's constant, Equation (15)
J = bubble flux, Equation (12)
k = overall frequency factor, Equation (14)
k_B = frequency factor for break up
k_C = frequency factor for coalescence
k_L = liquid side mass transfer coefficient
L = column length
N_B = bubble density, Equation (11)
P = pressure
p_L = partial pressure of CO_2 in liquid phase
Pe_L = liquid phase Peclet number, Equation (27)
Q = cross sectional area of column
R = gas constant
St_G = gas phase Stanton number, Equation (24)
St_L = liquid phase Stanton number, Equation (28)
u = superficial velocity
$\bar{u}_G$ = mean superficial gas velocity, Equation (9)
V = volume flow rate
x = CO_2 mole fraction in gas phase
z = dimensionless axial coordinate, h/L
α = pressure ratio, Equation (5)
β = function, def. by Equation (25)
ϕ = function, def. by Equation (2)
ϵ_G = gas hold up
$\bar{\epsilon}_G$ = mean gas hold up, Equation (3)
ρ = liquid density

Indices

0 = column bottom
$1, T$ = column top
i = inlet
G = gas
L = liquid

References

(1) Lücke, J., Oels, U. and Schügerl, K., 5th Int. Ferment. Symp., 1.01, Berlin (1976).
(2) Lehmann, J., Reuss, M. and Jefferis, R., 5th Int. Ferment. Symp., 5.08, Berlin (1976).
(3) Schügerl, K., Oels, U. and Lücke, J., Adv. Biochem. Eng., 7 1 (1977).
(4) Schügerl, K., Lücke, J., Lehmann, J. and Wagner, F., Adv. Biochem. Eng., 8, 63 (1978).
(5) Urza, I. and Jackson, M. L., Ind. Eng. Chem. Process Des. Dev. 14, 106 (1975).
(6) Edwards, L. L., Leber, B. P. and Jackson, M. L., Chem. Eng. Prog., Symp. Ser., Water 1975, 71, No. 151.
(7) Shulman, H. L. and Molstad, M. C., Ind. Eng. Chem. 42, 1058 (1950).
(8) Voyer, R. D. and Miller, A. I., Can. J. Chem. Eng. 46, 335 (1968).
(9) Chen, B. H. and Vallabh, R., Ind. Eng. Chem. Process Des. Dev. 9, 121 (1970).
(10) Coulon, G., Chem.-Ing.-Tech. 43, 280 (1971).
(11) Deckwer, W.-D., Burckhart, R. and Zoll, G., Chem. Eng. Sci. 29, 2177 (1974).
(12) Burckhart, R. and Deckwer, W.-D., Verfahrenstechn. (Mainz) 10, 429 (1976).
(13) Maclean, G. T., Erickson, L. E., Hsu, K. H. and Fan, L. T., Biotechnol. Bioeng. 19, 493 (1977).
(14) Pavlica, R. T. and Olson, J. H., Ind. Eng. Chem. 62, 45 (1970).
(15) Mhaskar, R. D., Chem Eng. Sci. 29, 897 (1974).
(16) Szeri, A., Shah, Y. T. and Madgavkar, A., Chem. Eng. Sci. 31, 225 (1976).
(17) Deckwer, W.-D., Chem. Eng. Sci. 31, 309 (1976).
(18) Deckwer, W.-D., Chem. Eng. Sci. 32, 51 (1977).
(19) Deckwer, W.-D., Zaidi, A. and Adler, I., Chem.-Ing.-Tech. 48, 1075 (1976).
(20) Kölbel, H., Beinhauer, R. and Langemann, H., Chem.-Ing.-Tech. 44, 697 (1972).
(21) Burckhart, R. and Deckwer, W.-D., Chem. Eng. Sci 30, 357 (1975).
(22) Akita, K. and Yoshida, F., Ind. Eng. Chem. Process Des. Dev. 12, 76 (1973).
(23) Gestrich, W. and Rähse, W., Chem.-Ing.-Tech. 47, 8 (1975).
(24) Kumor, A. Degaleesau, T. E., Laddha, G. S. and Hoelscher, H. E., Can. J. Chem. Eng. 54, 503 (1976).
(25) Friedlander, S. K. and Topper, L., Turbulence, Interscience Publ., New York 1961.
(26) Burckhart, R., Dr.-Ing. thesis, Technische Universität, Berlin, 1976.
(27) Calderbank, P. H. and Moo-Young, M. B., Chem. React. Eng. Proc. 3rd Eur. Symp. Amsterdam, 1964, p. 91.
(28) Lee, J. C. and Ssali, G. W. K., Joint Meeting of Bubbles and Foams, VTG/VDI-Inst. Chem. Eng., Nuremberg 1971, p. S1-6.1.
(29) Lockett, M. J. and Kirkpatrick, R. D., Trans. Inst. Chem. Eng. 53, 267 (1975).
(30) Deckwer, W.-D., Zaidi, A. and Adler, I., Preprints Eur. Congr.: Transfer Processes in Particle Systems, Nuremberg, Germany, 1977, ed. by H. Brauer and O. Molerus.
(31) Baird, H. M. I. and Rice, R. G., Chem. Eng. J. 9, 171 (1975).
(32) Subramanian, G. and Tien, C., Can. J. Chem. Eng. 53, 611 (1975).
(33) Towell, G. D. and Ackerman, G. H., Proc. ISCRE 2, B3-1, Amsterdam (1972).
(34) Lee, E. S., "Quasilinerization and Invariant Imbedding" Academic Press, New York 1968.
(35) Calderbank, P. H. and Moo-Young, M., Chem. Eng. Sci. 16, 39 (1961).
(36) Akita, K. and Yoshida, F., Ind. Eng. Chem. Process Dec. Dev. 13, 84 (1974).
(37) Reuss, M., Dr.-Ing. thesis, Technische Universität Berlin, (1970).
(38) Higbie, R., Trans. AIChE 35, 365 (1935).
(39) Hughmark, G. A., Ind. Eng. Chem. Process Des. Dev. 6, 218 (1967).

Manuscript received July 21, 1977; accepted for publication November 10, 1977.

★ ★ ★